SAND2018-7487C

Failure Thresholds in CBRAM Due to Total Ionizing Dose and Displacement Damage Effects

J. L. Taggart, *Student Member, IEEE*, R. B. Jacobs-Gedrim, *Member, IEEE*, M. L. McLain, *Member, IEEE*, H. J. Barnaby, *Fellow, IEEE*, E. S. Bielejec, *Member, IEEE*, W. Hardy, M. J. Marinella, *Member, IEEE*, M. N. Kozicki, K. Holbert, *Member, IEEE*

***Abstract*—.**

***Index Terms*—CBRAM, chalcogenide glass, conductive bridging, electrochemical metallization, nanoionic memory, memristors, radiation effects, dose effects, ionizing radiation, TID, displacement damage.**

I. Introduction

CONDUCTIVE bridging random access memory (CBRAM) is a non-volatile memory (NVM) with a high tolerance to total ionizing dose (TID). Its megarad tolerance to TID in addition to its potential to perform low power, high speed operations, has made CBRAM a technology of interest in the space industry [1], [2]. Further, more ambitious missions to environments such as Europa, require higher levels of radiation tolerance than what is required for Earth orbits and interstellar space travel [3]–[5]. Researching and developing technologies that can survive the gas giants' radiation environments will be crucial to the success of those missions. In these extreme environments, electronics can be exposed to tens of Mrad(Si) over a matter of months in addition to displacement damage due to the heavier high energy ions trapped in the magnetosphere [3]. It is now relevant and necessary to examine the thresholds of radiation tolerance in CBRAM devices as well as begin to delve into the mechanism responsible for observed radiation effects.

CBRAM has been shown to be TID tolerant up to 10 Mrad($Ge_{30}Se_{70}$) for Ag-$Ge_{30}Se_{70}$ devices [6]–[8] and 7.1 Mrad(SiO_2) for Cu-SiO_2 devices [9], [10]. Recent investigations into displacement damage (DD) effects indicate some sensitivity to 14 MeV neutrons during device programming at high fluences in the order of 10^{13} n/cm^2 [11]. The same study provided a preliminary study of heavy ion effects using 200 keV Si ion exposures. The heavy ion study found that Ag-$Ge_{30}Se_{70}$ devices experienced changes in resistance state at high fluences of 4.2×10^{13} ions/cm^2, with irrecoverable failure after 1.7×10^{14} ions/cm^2. The previous ion experiment used a fluence beyond the threshold required to induce a resistance state change with the intent of examining possible sensitive regions of the CBRAM cell. In this current work, the 200 keV Si ion irradiations are performed again to determine the lowest fluence necessary to induce a resistance change. In addition to Si ions, 100 keV Li, and 1 MeV Ta irradiations were performed to compare TID and displacement damage effects based on the differences in respective linear energy transfer (LET) and nonionizing energy loss (NIEL).

Heavy ion testing has been performed on HfO_2 [12], TaOx and TiO_2 [13]–[15] valence change memories. Valence change memory is a filamentary resistive memory technology similar to CBRAM [16]. During ion bombardment, the resistance state of the metal-oxide devices was shown to decrease after a fluence threshold. The failure in those studies was attributed to an increase in oxygen vacancies that increased the number of conductive paths between the terminals. For CBRAM devices, this work will show that a similar decrease in resistance is observed, but the mechanism responsible for resistance change is not yet known.

CBRAM is a two-terminal electrochemical resistive memory where the resistive state is controlled by the formation of a metallic filament bridging the two terminals [17]. A CBRAM device is a three-layer material stack with a bottom cathode contact made from an inert metal, typically Ni or W, a solid electrolyte layer formed by doping $Ge_{30}Se_{70}$ with a reactive metal, such as Ag or Cu, and a top anode contact of the same reactive metal. When a positive voltage is applied to the anode the reactive metal oxidizes, creating cations that migrate through the electrolyte to the cathode contact where the metal ion is reduced [18]. While the bias is maintained the cations

The project or effort depicted was or is sponsored by the Department of the Defense, Defense Threat Reduction Agency under grant no. HDTRA1-17-1-0038 and by the Air Force Research Laboratory Det 8/RVKVE under grant no. FA9452-13-1-0288. Sandia National Laboratories is a multimission laboratory managed and operated by National Technology and Engineering Solutions of Sandia, LLC., a wholly owned subsidiary of Honeywell International, Inc., for the U.S. Department of Energy's National Nuclear Security Administration under contract DE-NA-0003525.

J. L. Taggart is with the School of Electrical, Computer and Energy Engineering, Arizona State University, Tempe, AZ 85287-5706, USA (e-mail: jennifer.taggart@asu.edu).

R. B. Jacobs-Gedrim, M. L. McLain, E. S. Bielejec, W. Hardy, and M. J. Marinella are with Sandia National Laboratories, Albuquerque, NM 87123, USA

H. J. Barnaby, M. N. Kozicki, and K. Holbert are with the School of Electrical, Computer and Energy Engineering, Arizona State University, Tempe, AZ 85287-5706, USA

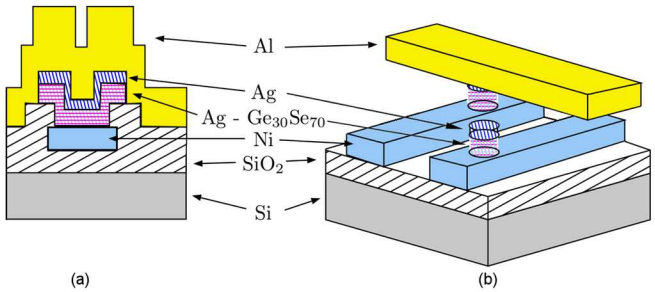

Fig. 1 (a) Material stack of the CBRAM crossbar devices and (b) the cutaway representation of the crossbars.

from the anode continue to migrate and form a filament from the cathode to the anode. The low resistance state (LRS) of the device is defined by the resistance of the formed conductive filament. Reversing the bias reverses the reduction-oxidation process and dissolves the filament back to the anode contact. The resistance between the two terminals with no filament present is the high resistance state (HRS).

During the operation of non-volatile memory, a device can be written to, read from, or sit idle, retaining a programmed state. To best understand how radiation can affect the performance, each of the operations need to be tested while in a radiation environment. NVM typically spends much of its life retaining a state. In the following work, the retention of a programmed retention state and the programming window, extracted from DC cycling, is tested with increasing ion fluence. Testing was performed with 100 keV Li, 200 keV Si and 1 MeV Ta ions. For DC cycling testing, only 100 keV Li test were performed and the results are compared to retention testing and previous neutron tests performed with DC cycling [11]. TID and DD were then calculated at the ion fluences where failure occurred. Section II provides the fabrication process used to create the CBRAM crossbar devices. Section III describes the electrical measurements performed for retention of state testing and DC cycling tests and includes details on the fluence steps used during irradiation. Section IV presents the results of CBRAM during the heavy ion exposures. Section V compares the TID and DD effect and discusses properties of the chalcogenide system that could contribute to the effects observed. Section VI provides a conclusion with a brief highlight of key findings.

II. Fabrication

CBRAM devices were fabricated in the NanoFab cleanroom at Arizona State University. The crossbar devices were fabricated in the following manner. A 525 µm Si wafer was coated in 104 nm of SiO_2 using plasma enhanced chemical vapor deposition (PECVD). The SiO_2 layer provides electrical isolation of the CBRAM array from the Si wafer. The 65 nm Ni cathode contacts were deposited using electron beam evaporation in a Lesker PVD75. The Ni layer was patterned using photoresist and wet etched using Nickel Etchant TFB to create the bottom bar feature. The device isolation layer was created by coating the cathode contacts in 96 nm of PECVD SiO_2. Circular features were etched through the SiO_2 layer down to the Ni contacts by patterning a double layer resist and etching the SiO_2 using an anisotropic reactive ion etch (RIE) in

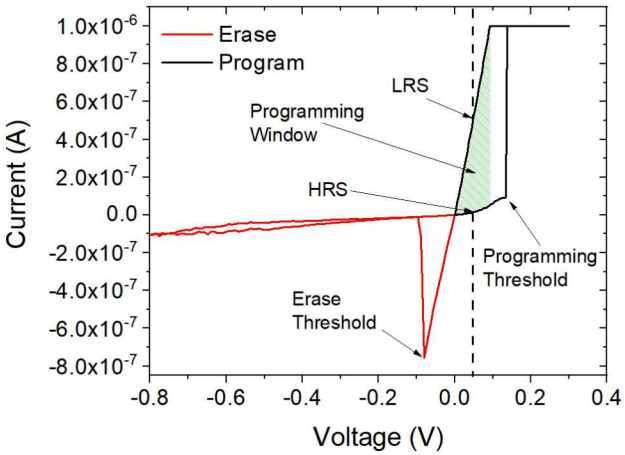

Fig. 2 Typical I-V curve of a CBRAM cell. HRS/LRS programming window is defined as the ratio between the HRS and LRS in the region below the programming threshold.

a Plasmatherm 790. The wafer was patterned with a double layer lift-off resist (LOR) and the switching layer of the devices was created using thermal evaporation in a Cressington 308R. First, 65 nm of $Ge_{30}Se_{70}$ was evaporated followed by 30 nm of Ag. The wafer was removed from vacuum and placed under a 3.26 mW UV source for 27 minutes to photodope the Ag into the $Ge_{30}Se_{70}$ layer [19]. Studies of photodiffusion in $Ge_{30}Se_{70}$ systems suggest that the Ag concentration is saturated at 33 at.% [20]. The wafer was placed back in the Cressington and an additional 35 nm of Ag was deposited. The resist was dissolved in acetone to lift-off the excess material, leaving behind the CBRAM cells in the holes etched through the SiO_2. The top anode contacts were patterned with LOR and 350 nm of Al was sputtered using a Lesker PVD75. The excess Al was lifted off in acetone to create the Al crossbar. The full device stack is shown in Fig. 1. Devices prepared for Ta and Si ion irradiation exposures do not have an overlaying Al layer and were fabricated in the method described in [11].

III. Experiment Setup

All heavy ion irradiations were performed at the Ion Beam Laboratory (IBL) at Sandia National Laboratories (SNL). ^{60}Co γ-ray irradiations were performed at the Gamma Irradiation Facility (GIF) also located at SNL. Prior to testing, the devices were cycled with a DC current-voltage (I-V) sweep using an Agilent B1500 to verify that the devices operated correctly. Each device was programmed with a 10 mV staircase sweep from 0 V to 0.3 V and back to 0 V and erased with a sweep from 0 V to -0.8 V back to 0V. Typically, five to ten initial sweeps are performed.

A. 100 keV Li^+ Ion Beam Exposures

CBRAM crossbars with 5 µm diameter circular devices were used for the Li ion irradiations. Exposures were performed using the NanoImplanter (NI) raster scanning focused ion beam. Prior to exposure the devices were placed under vacuum in the NI and probed and I-V measurements performed. Two different measurements were performed. The first set of testing

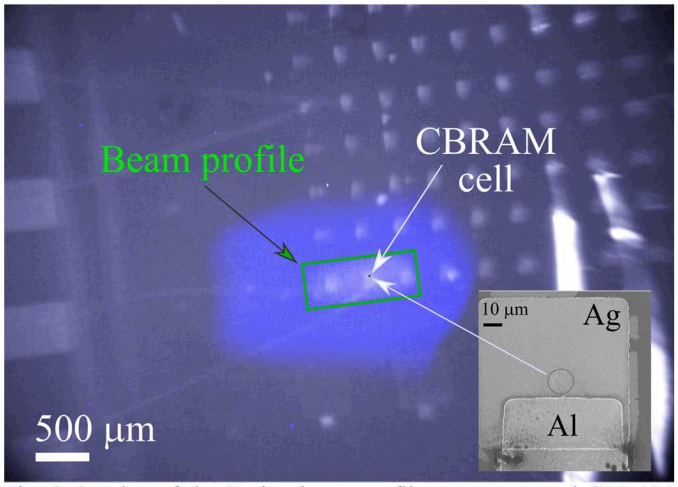

Fig. 3 Overlay of the Ta-ion beam profile on an exposed CBRAM device. The green square marks the profile of the Ta beam and the red dot with white arrow marks the location of a tested device. The bottom right inset shows the device in higher detail.

examined the retention of a programmed resistive state to an increasing fluence of ions. The second test looked at how the programming window of a device evolved with increasing fluence. Fig. 2 depicts the definition of the programming window as well as marks the HRS and LRS of a typical I-V sweep. For the state retention testing, three devices were erased into an HRS and three were programmed to an LRS with a 10 µA compliance current. A small (sub programming threshold) DC I-V read sweep from 0 V to 30 mV was used to sample the resistive state of the device before irradiation. Each device was exposed and tested individually. The 40 nm diameter Li beam was raster scanned in 40 nm steps over a 25 µm × 25 µm area over each device to a fluence of 10^{11} ions/cm^2. The device remained probed during irradiation with no bias applied. After irradiation, the 30 mV read sweep was applied to measure the state of the device. Exposures were continued in 10^{11} ions/cm^2 fluence steps to 10^{12} ions/cm^2 where the fluence was increased to 10^{12} ions/cm^2 steps and at 10^{13} ions/cm^2 the step was increased to 10^{13} ions/cm^2. A read sweep was performed on the device after each fluence step. The devices were irradiated up to a total fluence of 5×10^{13} ions/cm^2 or until the device shorted.

Two devices were used to examine the response of the HRS/LRS programming window to ion bombardment. Prior to exposure, each device was DC cycled and left in the HRS. The state was read with a 30 mV DC sweep before exposure. After each fluence step, a DC read was performed followed by a DC cycle then another DC read prior to the next irradiation. A 10^{12} ions/cm^2 fluence step was used for each irradiation up to a total fluence of 3×10^{13} ions/cm^2 or until the device failed to switch. The HRS and LRS were extracted from the I-V curve at the 30 mV point.

B. 200 keV Si^{2+} Ion Beam Exposures

Six 5 µm diameter circular CBRAM devices with an offset Al contact, similar to the device in the inset of Fig. 3, were tested. Two devices were tested in a HRS and the remaining four were programmed to the LRS using a 25 µA compliance. The devices were from the same wafer as the crossbar structures used for Li-ion testing. It was necessary to use devices with no direct Al overlayer, as the 350 nm Al layer was too thick to allow 200 keV Si ions to penetrate to the electrolyte layer. Si-ion exposures were performed in the same manner as Li-ion testing. Prior to testing, each device was DC cycled to verify that the device was functional. At the start of the test, each device was programmed to either an HRS or LRS and the status of its resistive state was measured at each fluence step using a 30 mV DC sweep.

C. 1 MeV Ta^{2+} Ion Beam Exposure – 10 µm discreet devices

Three devices were irradiated with Tandem accelerated 1 MeV Ta ions. The devices tested were those described in [6] with the Al contact offset from the area of the CBRAM cell; as depicted in Fig. 3. The devices were wire bonded in a 24 pin DIP and placed on a circuit board inside the beam line with BNC accessible connections to an Agilent 4155 parameter analyzer. Two of the devices were DC cycled and erased into an HRS while the third device was cycled and programmed into an LRS with a 10 µA compliance current. The Ta ion beam was approximately 500 µm × 1000 µm and fully covered the device area, as shown in the beam profile overlay in Fig. 3. During each exposure, a 50 mV read bias was applied to the anode contact with the cathode grounded.

D. SRIM calculations

The Stopping and Range of Ions in Materials (SRIM) [21] was used to calculate the deposited TID (rad) and displacement damage dose (MeV/g) due to ion bombardment. To perform the calculation, the ion ranging tables were generated from SRIM for each ion in each material used in the CBRAM fabrication. The LET and NIEL values were noted as the ion entered, passed through, and left the material layer. The starting ion energy, as the ion entered the next layer, was the final energy as it left the previous layer. The dose listed in the following results is the mean deposed dose in the chalcogenide switching layer (Ag-$Ge_{30}Se_{70}$). The LET and NIEL values generated from SRIM were converted to TID and DDD using the following equations,

$$TID\ [\mathrm{rad}] = LET \cdot \Phi \cdot K \quad (1)$$

$$DDD\ [\mathrm{MeV \cdot g^{-1}}] = NIEL \cdot \Phi \quad (2)$$

where $K = 1.6 \times 10^{-8}\ \mathrm{rad \cdot g \cdot MeV^{-1}}$ and Φ is the fluence in ions/cm^2.

E. ^{60}Co γ-ray in situ Exposure

Two packages of CBRAM crossbar devices were irradiated at the GIF for a total of 12 tested devices. Each package was irradiated separately. During exposure, the package under test was placed onto a printed circuit board (PCB) that allowed ribbon cable connection to outside the gamma cell. The PCB was encased in a Pb-Al enclosure to filter out low energy photons. CaF_2 thermoluminescent dosimeters (TLD) were placed around the package to measure and calculate the dose received at the device. Each package was irradiated at a dose rate of ~475 rad(Si)/s. The first package, containing 4 devices, was irradiated to 22.8 Mrad($Ge_{30}Se_{70}$) while the second package was irradiated to 23.9 Mrad($Ge_{30}Se_{70}$). A temperature probe was used inside the enclosure to monitor any significant heating during exposure.

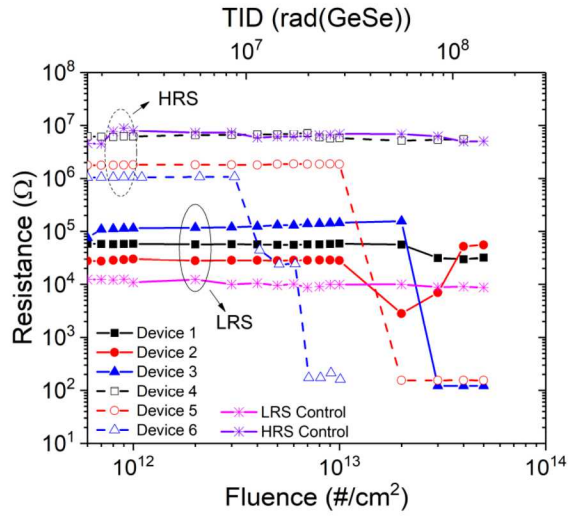

Fig. 4 Resistive state of CBRAM devices during 100 keV Li bombardment.

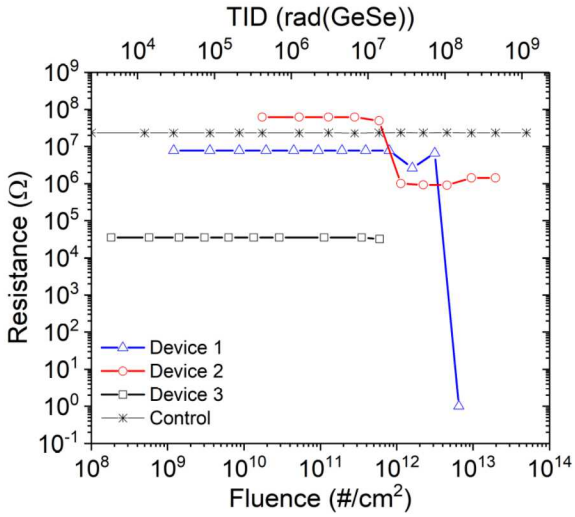

Fig. 5 Resistive state of CBRAM devices during 1 MeV Ta-ion bombardment.

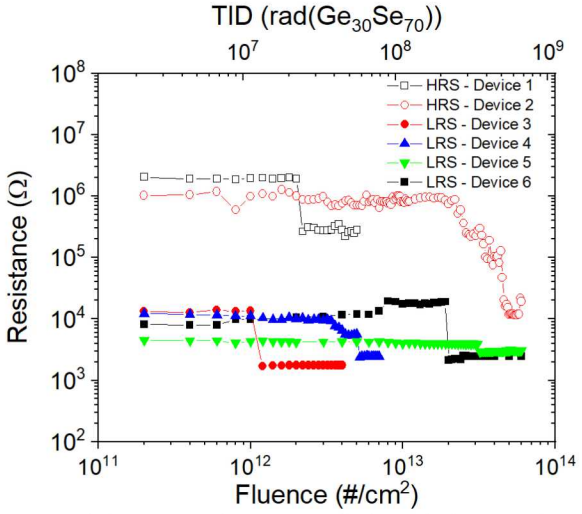

Fig. 6 Resistive state of CBRAM devices during 200 keV Si-ion bombardment.

During exposure, a 50 mV read bias was applied to the anode of each device, while grounding the cathode. The respective resistive states were monitored *in situ* using a Yokogawa DL850E. Of the 12 devices tested, 7 were programmed to an LRS and 5 to an HRS. A third package containing 2 HRS and 2 LRS control devices was tested outside of the gamma cell. The states of the control devices were monitored using the Yokogawa. Prior to exposure, all devices were DC I-V cycled 5 times to verify the operation and switching capability of each device.

IV. Results

A. State Retention During Heavy Ion Bombardment

For the Li ion exposure, three devices were initially set to an HRS while three others were set to an LRS. The resistance state of the six devices versus the accumulative Li ion fluence is shown in Fig. 4. The TID calculated using SRIM is marked on the top x-axis. Devices programmed to an HRS are plotted with dotted lines while the devices set to an LRS are solid lines. Of the devices programmed to an LRS only device 3 shorted after a fluence of 3×10^{13} ions/cm^2. Devices 1 and 2 failed to retain their initial state after a fluence of 10^{13} ions/cm^2 but they did not short. For the three devices programmed to an HRS devices 5 and 6 were shorted to an LRS. Device 5 shorted at a fluence of 2×10^{13} ions/cm^2. Device 6 decreased in resistance after a fluence of 3×10^{12} ions/cm^2 and shorted after 3×10^{12} ions/cm^2. Device 4 did not transition to an LRS but decreased slightly in resistance after a fluence of 10^{13} ions/cm^2.

The post resistance state after each pulse versus accumulative fluence is plotted in Fig. 5 for the 1 MeV Ta-ion exposure. Devices 1 and 2 were set to an HRS prior to exposure and device 3 was set to the LRS. Both devices in the HRS transitioned to a lower resistance after a fluence of 10^{12} ions/cm^2 and $3\text{x}10^{12}$ ions/cm^2 for devices 2 and 1, respectively. The device in an LRS was only tested up to 6×10^{11} ions/cm^2 with no notable change in resistance observed.

The results of the 200 keV Si ion exposure is shown in Fig. 6. All six devices tested showed a decrease in resistance at fluences above 10^{12} ions/cm^2. HRS device 1 decreased in resistance at 2×10^{12} ions/cm^2 and LRS devices 3 and 4 decreased at 10^{12} ions/cm^2 and 3.4×10^{12} ions/cm^2 respectively. HRS device 2 and LRS devices 5 and 6 did not decrease until and 2×10^{13} ions/cm^2. Unlike the state transition of device 1, once the resistive state of device 2 began to decrease, the change was gradual with increasing fluence.

B. DC Current-Voltage Cycling

Each device was DC cycled once after each fluence step. During exposure the device was left in the HRS. Fig. 7 shows how the HRS/LRS programming window collapsed after a fluence of 10^{13} ions/cm^2. Fig. 8 shows the measured HRS and LRS for both devices for each I-V sweep performed. Though both devices were located on the same die, device 1 was capable of switching with an HRS/LRS ratio 10x that of device 2. Since the LRS for a given compliance can be consistently set in radiation free lab conditions, the variation in the programming window is typically a result of variance in the HRS [7], [22]. The 10x HRS variation between device 1 and 2 is shown in Fig.

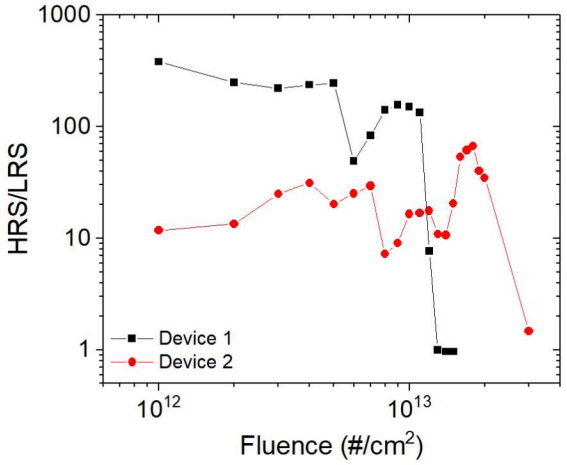

Fig. 7 HRS/LRS programming ratio for the I-V sweep performed after each 100 keV Li ion fluence step.

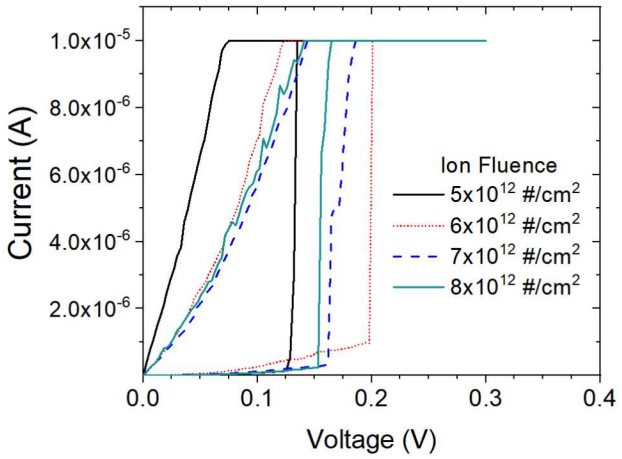

Fig. 9 Programming I-V sweeps of Device 1 at fluence steps where the resistance was observed to increase.

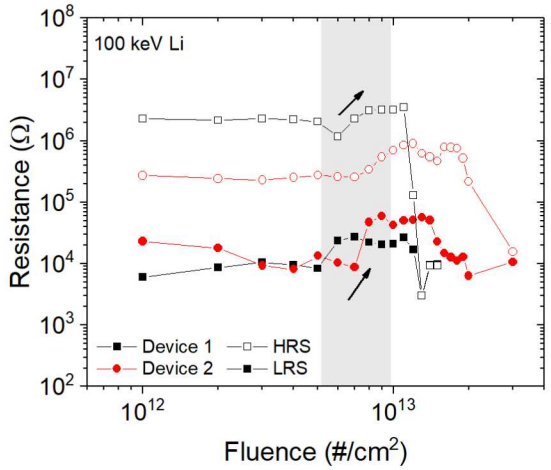

Fig. 8 Extracted HRS and LRS values for each device at each fluence step. Gray region highlights a trend where the resistance of both the HRS and LRS increased prior to shorting. Black curve with square symbols represents device 1 while the red curve with circular markers is device 2.

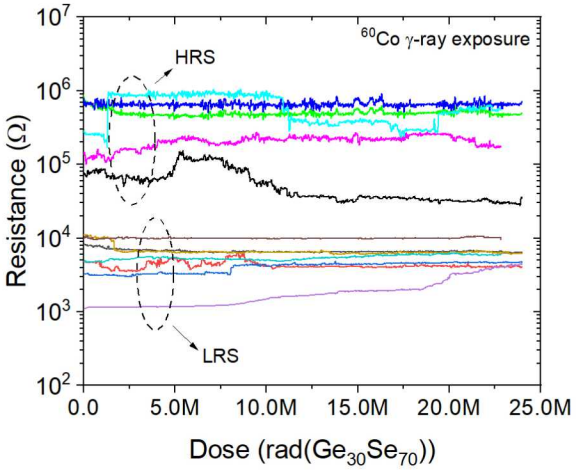

Fig. 10 Retention of state of 12 CBRAM devices observed *in situ* during ^{60}Co γ-ray irradiation.

8. This HRS variance is a typical phenomenon observed in these research quality CBRAM devices.

The gray region of Fig. 8 highlights an interesting trend where the HRS and LRS of both devices increased prior to the HRS collapsing to the LRS value (shorted). Fig. 9 displays the programming sweeps of device 1 marked in the gray area. In this region, the ohmic LRS response is shown to become less linear with increasing fluence. The ragged profile of the LRS curve suggests that ion migration is occurring within the filament structure resulting in spikes of conductivity. Non-irradiated CBRAM devices have limited ion movement at voltages below the programming threshold, allowing for their non-volatile behavior. The nonlinear response, in addition to the variation in programming threshold, provides evidence that electrolyte region of the device has changed in such a way to affect Ag migration.

C. Retention of State During ^{60}Co TID Exposure

Ion irradiations result in a combined environment of ionizing radiation and nonionizing energy loss with the potential to cause displacement damage. Separating effects due purely to TID versus displacement damage is a tricky process unless the mechanism responsible for the observed failures is known. To examine the potential for TID effects, γ-ray testing using ^{60}Co was performed up to 23.9 Mrad($Ge_{30}Se_{70}$). Fig. 10 shows the *in situ* response of the 7 devices programmed to an LRS and the 5 devices programmed to HRS. Throughout the 16 hour exposure, several devices did drift from their initial resistance state but all devices maintained their relative binary state (no switch from HRS or LRS or vice versa). One HRS device, shown as the back curve, did drift toward the LRS state but did not experience a sudden transition, such as those observed during ion testing. This HRS device also started in a lower than typical HRS state, most likely due to a partially formed filament.

V. Discussion

Using the doses calculated from SRIM, Fig. 11 was constructed to assess if TID or DDD played the greater role in the observed radiation effects during retention testing. Using the point at which the resistance reduced by more than a half decade, the TID and DDD were calculated at the fluence step prior to failure. At failure, the 1 MeV Ta ions are shown to produce 6 times the DDD as 200 keV Si and 10 times the DDD as the 100 keV Li ions though most devices experienced resistance decreases within the same magnitude of TID. This strongly suggests that the observed changes were a result of TID. However, three devices exposed to Si ions did not fail until higher fluences and one device in an HRS exposed to Li ions did not fail during the fluences tested. To test for effects due purely to TID, the ^{60}Co γ-ray exposures were performed up to 24 Mrad($Ge_{30}Se_{70}$). During those exposures, as shown in Fig. 10, there were no drastic decreases in resistive state. Four of the 15 devices exposed to heavy ions were shown to exhibit changes in resistance by 24 Mrad($Ge_{30}Se_{70}$). Further TID testing beyond 50 Mrad($Ge_{30}Se_{70}$) may be needed to conclusively state whether or not TID alone can cause a failure of retained state. The stability of the CBRAM during TID testing in addition to the higher fluence threshold seen during Si ion testing, implies that DDD may also contribute to the observed effects.

DC I-V sweeps were performed to observe the behavior of device programming during ion bombardment. DC sweeps provide insight into device characteristics that are useful for determining how filament growth is affected during radiation exposure. The gray region of Fig. 8 highlights the fluences where the I-V characteristic of a CBRAM devices began to distort prior to the collapse of the HRS/LRS window. The programming sweeps in Fig. 9 show that the LRS region becomes less linear with increasing fluence, indicating that the conduction mechanism along the filament path is evolving. Typically the LRS region is near ohmic due to the metallic filament spanning the two electrodes [1], [18]. Actual conduction along the filament has been found to be regulated by quantum point contact like confinement at narrow points in the filament [23], [24]. In some cases, particularly in Cu-SiO_2 devices, the LRS region can become non-linear due to partial filament dissolution as the electric field across the terminals decreases during the sweep [10]. The dissolution could be due to a reduction in ion supply, preventing the filament from forming fully.

For Se-rich glasses ($x < 0.33$ in Ge_xSe_{1-x}) Ag behaves as a network modifier, forming Ag_2Se crystalline phases throughout the chalcogenide glass network [25], [26]. The Ag_2Se nanocrystals behave as fast ion conductors, facilitating the hopping of Ag^+ cations through the chalcogenide glass [25], [26]. ^{60}Co irradiations of bulk $Ag_y(Ge_xSe_{1-x})_{1-y}$ films to 5 Mrad show that ionizing radiation creates β-Ag_2Se crystalline phases while slightly diminishing the number of α-Ag_2Se phases [27]. The β-Ag_2Se crystalline phase is orthorhombic and have a lower ionic conductivity than the cubic α phase [26]–[28]. The β phase typically forms 8 nm nanocrystals while α phase crystals are around 5 nm. The distance between these nanocrystals are 1.5 nm on average [18]. The nanocrystals can act as nucleation sites for filament growth with the dominate

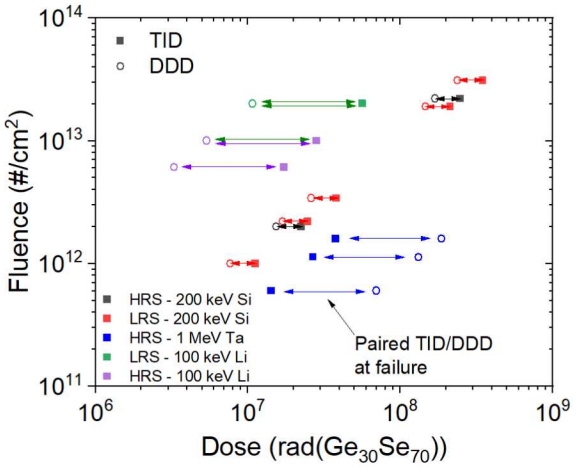

Fig. 11 TID (solid marker) and DDD (open maker) in devices when resistance state observed to decrease due to irradiation. For a given ion fluence, the respective TID and DDD are marked with an arrow between them.

filament path dictated by local fields and sufficient ion supply. A completed bridging filament, from cathode to anode, will be a connect-the-dots structure between the smaller filament structures forming on the nanocrystals [18]. The distance between nanocrystals is small enough to allow tunneling current. In cases where Ag supply is insufficient to complete a continuous filament, current in the LRS is dominated by the tunneling between nucleation sites.

Failure occurred for DC cycling within the same fluence range as retention testing of the 100 keV Li ion exposure. The similar fluence threshold indicates that the failure mechanism may be the same for both tests. Based on DC sampling taken pre and post each fluence step, at failure, the devices were observed to short prior to the I-V sweep being performed. After shorting, many devices could be partially erased after several erase sweeps, indicating that the short was due to an introduction of Ag and not due to a material change resulting in a permanent conductive path. It is not yet clear what mechanism is responsible for the introduction of excess Ag. At high TID, Ag may be introduced via local fields created from carrier generation. The introduction of excess Ag into the chalcogenide layer could also be due to displacement damage and mixing at the Ag/chalcogenide interface. Kinetic ion interactions could also release Ag bound to the Ag_2Se compounds, creating a supply of mobile Ag ions within the chalcogenide layer. Further material analysis is necessary to determine how the switching layer is evolving at these higher doses of radiation.

VI. Conclusion

The response of Ag-$Ge_{30}Se_{70}$ CBRAM to 100 keV Li, 1 MeV Ta, and 200 keV Si ion irradiations was examined. In all irradiations the programmed resistance state of the CBRAM devices were seen to decrease after a certain fluence. The TID and DDD in the Ag-$Ge_{30}Se_{70}$ switching layer was calculated for each exposure at the point where the resistance state decreased. The TID and DDD threshold of each device was compared and it was found that TID was more highly correlated than DDD, suggesting that TID was the main cause

of failure. ^{60}Co retention testing to 24 Mrad($Ge_{30}Se_{70}$) showed no abrupt failure, indicating that failure during ion testing may be a synergistic response to the combined environment.

VII. Acknowledgements

The authors would like to thank Jacob Calkins and Art Edwards for their support of this work.

VIII. References

[1] M. N. Kozicki and H. J. Barnaby, "Conductive bridging random access memory—materials, devices and applications," IOP Publishing, 2016.

[2] Y. Gonzalez-Velo, H. J. Barnaby, and M. N. Kozicki, "Review of radiation effects on ReRAM devices and technology," *Semicond. Sci. Technol.*, vol. 32, no. 8, p. 083002, Aug. 2017.

[3] M. Cherng, I. Jun, and T. Jordan, "Optimum shielding in Jovian radiation environment," *Nucl. Instruments Methods Phys. Res. Sect. A Accel. Spectrometers, Detect. Assoc. Equip.*, vol. 580, no. 1, pp. 633–636, Sep. 2007.

[4] M. C. Casey, A. J. Boutte, M. J. Campola, M. A. Carts, E. P. Wilcox, C. J. Marshall, A. M. Phan, J. A. Pellish, W. A. Powell, and M. A. Xapsos, "A Comparison of High-Energy Electron and Cobalt-60 gamma-Ray Radiation Testing," in *2012 IEEE Radiation Effects Data Workshop*, 2012, vol. 60, pp. 1–5.

[5] S. Bourdarie and M. A. Xapsos, "The Space Radiation Environment," vol. 55, no. 4, pp. 1810–1832, 2008.

[6] Y. Gonzalez-Velo, A. Mahmud, W. Chen, J. L. Taggart, H. J. Barnaby, M. N. Kozicki, M. Ailavajhala, K. E. Holbert, and M. Mitkova, "Radiation hardening by process of CBRAM resistance switching cells," *IEEE Trans. Nucl. Sci.*, vol. 63, no. 4, pp. 2145–2151, Aug. 2016.

[7] Y. Gonzalez-Velo, H. J. Barnaby, M. N. Kozicki, P. Dandamudi, A. Chandran, K. E. Holbert, M. Mitkova, and M. Ailavajhala, "Total-ionizing-dose effects on the resistance switching characteristics of chalcogenide programmable metallization cells," *IEEE Trans. Nucl. Sci.*, vol. 60, no. 6, pp. 4563–4569, 2013.

[8] J. L. Taggart, Y. Gonzalez-Velo, D. Mahalanabis, A. Mahmud, H. J. Barnaby, M. N. Kozicki, K. E. Holbert, M. Mitkova, K. Wolf, E. Deionno, and A. L. White, "Ionizing Radiation Effects on Nonvolatile Memory Properties of Programmable Metallization Cells," *IEEE Trans. Nucl. Sci.*, vol. 61, no. 6, pp. 2985–2990, Dec. 2014.

[9] W. Chen, H. J. Barnaby, M. N. Kozicki, A. H. Edwards, Y. Gonzalez-Velo, R. Fang, K. E. Holbert, S. Yu, and W. Yu, "A Study of Gamma-Ray Exposure of Cu–SiO2 Programmable Metallization Cells," *IEEE Trans. Nucl. Sci.*, vol. 62, no. 6, pp. 2404–2411, Dec. 2015.

[10] W. Chen, R. Fang, H. J. Barnaby, M. B. Balaban, Y. Gonzalez-Velo, J. L. Taggart, A. Mahmud, K. Holbert, A. H. Edwards, and M. N. Kozicki, "Total-Ionizing-Dose Effects on Resistance Stability of Programmable Metallization Cell Based Memory and Selectors," *IEEE Trans. Nucl. Sci.*, vol. 64, no. 1, pp. 269–276, 2017.

[11] J. L. Taggart, R. Fang, Y. Gonzalez-Velo, H. J. Barnaby, M. N. Kozicki, J. L. Pacheco, E. S. Bielejec, M. L. McLain, N. Chamele, A. Mahmud, and M. Mitkova, "Resistance State Locking in CBRAM Cells Due to Displacement Damage Effects," *IEEE Trans. Nucl. Sci.*, vol. 64, no. 8, pp. 2300–2306, 2017.

[12] S. L. Weeden-Wright *et al.*, "TID and displacement damage resilience of 1T1R HfO2Resistive Memories," *IEEE Trans. Nucl. Sci.*, vol. 61, no. 6, pp. 2972–2978, 2014.

[13] D. R. Hughart, A. J. Lohn, P. R. Mickel, S. M. Dalton, P. E. Dodd, M. R. Shaneyfelt, A. I. Silva, E. Bielejec, G. Vizkelethy, M. T. Marshall, M. L. Mclain, and M. J. Marinella, "A Comparison of the Radiation Response of TaOx and TiO2 Memristors," *IEEE Trans. Nucl. Sci.*, vol. 60, no. 6, pp. 4512–4519, 2013.

[14] F. Tan, R. Huang, X. An, Y. Cai, Y. Pan, W. Wu, H. Feng, X. Zhang, and Y. Wang, "Investigation on the response of TaOx-based resistive random-access memories to heavy-ion irradiation," *IEEE Trans. Nucl. Sci.*, vol. 60, no. 6, pp. 4520–4525, 2013.

[15] H. J. Barnaby, S. Malley, M. Land, S. Charnicki, A. Kathuria, B. Wilkens, E. DeIonno, and W. M. Tong, "Impact of Alpha Particles on the Electrical Characteristics of TiO2 Memristors," *IEEE Trans. Nucl. Sci.*, vol. 58, no. 6, pp. 2838–2844, Dec. 2011.

[16] R. Waser, R. Dittmann, C. Staikov, and K. Szot, "Redox-based resistive switching memories nanoionic mechanisms, prospects, and challenges," *Adv. Mater.*, vol. 21, no. 25–26, pp. 2632–2663, 2009.

[17] I. Valov and M. N. Kozicki, "Cation-based resistance change memory," *J. Phys. D. Appl. Phys.*, vol. 46, no. 7, p. 074005, Feb. 2013.

[18] M. N. Kozicki and M. Mitkova, "Mass transport in chalcogenide electrolyte films – materials and applications," *J. Non. Cryst. Solids*, vol. 352, no. 6–7, pp. 567–577, May 2006.

[19] A. V. Kolobov and S. R. Elliott, "Photodoping of amorphous chalcogenides by metals," *Adv. Phys.*, vol. 40, no. 5, pp. 625–684, 1991.

[20] M. Mitkova and M. N. Kozicki, "Silver incorporation in Ge-Se glasses used in programmable metallization cell devices," *J. Non. Cryst. Solids*, vol. 299–302, no. PART 2, pp. 1023–1027, 2002.

[21] J. F. Ziegler, M. D. Ziegler, and J. P. Biersack, "SRIM - The stopping and range of ions in matter (2010)," *Nucl. Instruments Methods Phys. Res. Sect. B Beam Interact. with Mater. Atoms*, vol. 268, no. 11–12, pp. 1818–1823, 2010.

[22] D. Kamalanathan, A. Akhavan, and M. N. Kozicki, "Low voltage cycling of programmable metallization cell memory devices," *Nanotechnology*, vol. 22, no. 25, p. 254017, Jun. 2011.

[23] A. Belmonte, U. Celano, A. Redolfi, A. Fantini, R. Muller, W. Vandervorst, M. Houssa, M. Jurczak, and L. Goux, "Analysis of the Excellent Memory Disturb Characteristics of a Hourglass-Shaped Filament in Al_2O_3/Cu-Based CBRAM Devices," *IEEE Trans. Electron Devices*, vol. 62, no. 6, pp. 2007–2013, Jun. 2015.

[24] J. R. Jameson, N. Gilbert, F. Koushan, J. Saenz, J. Wang, S. Hollmer, and M. Kozicki, "Effects of cooperative ionic motion on programming kinetics of conductive-bridge memory cells," *Appl. Phys. Lett.*, 2012.

[25] M. Mitkova, Y. Wang, and P. Boolchand, "Dual chemical role of Ag as an additive in chalcogenide glasses," *Phys. Rev. Lett.*, vol. 83, no. 19, pp. 3848–3851, 1999.

[26] S. ya Miyatani, "Ionic conductivity in silver chalcogenides," *J. Phys. Soc. Japan*, vol. 50, no. 10, pp. 3415–3418, 1981.

[27] M. S. Ailavajhala, Y. Gonzalez-Velo, C. Poweleit, H. Barnaby, M. N. Kozicki, K. Holbert, D. P. Butt, and M. Mitkova, "Gamma radiation induced effects in floppy and rigid Ge-containing chalcogenide thin films," *J. Appl. Phys.*, vol. 115, no. 4, p. 043502, Jan. 2014.

[28] F. Kirchhoff, J. M. Holender, and M. J. Gillan, "Structure, Dynamics and Electronic Structure of Liquid Ag-Se Alloys Investigated by Ab Initio Simulation," *Phys. Rev. B*, vol. 54, no. 1, p. 14, 1996.